THE STATISTICAL PHYSICS OF SEDIMENTARY ROCK

The complexity of million-year-old sedimentary rock is being unraveled by such modern concepts of random systems as fractals, percolation and diffusion-limited growth.

Po-zen Wong

I ascribe to nature neither beauty, deformity, order nor confusion. It is only from the viewpoint of our imagination that we say that things are beautiful or unsightly, orderly or chaotic

-Baruch Spinoza, 1665

Sedimentary rock makes up much of the Earth's surface and contains two of the most vital fluids for our lives—water and hydrocarbons. Yet physicists have paid little attention to rock, mainly because we are discouraged by its apparent complexity. We are well trained in working with idealized models, but when faced with a piece of rock, not only do we not know where to begin, but we also may question whether it is even possible to find interesting physics in such a "dirty" and uncontrolled system. With further thought, however, we should realize that these are but the usual mental barriers that we have to overcome every time we study something new.

In the last few years, physicists who have ventured into this unfamiliar territory have gained new insight into sedimentary rock using concepts of statistical physics.1 The threat of an energy crisis and the once seemingly everrising price of oil provided both the incentive and the resources to take an unconventional look at rock, because an understanding of the basic physics of rock promises to improve the science and technology used in the oil industry. In this article I describe a few problems related to the structural and transport properties of rock and in particular the flow patterns of oil and water (figure 1) that

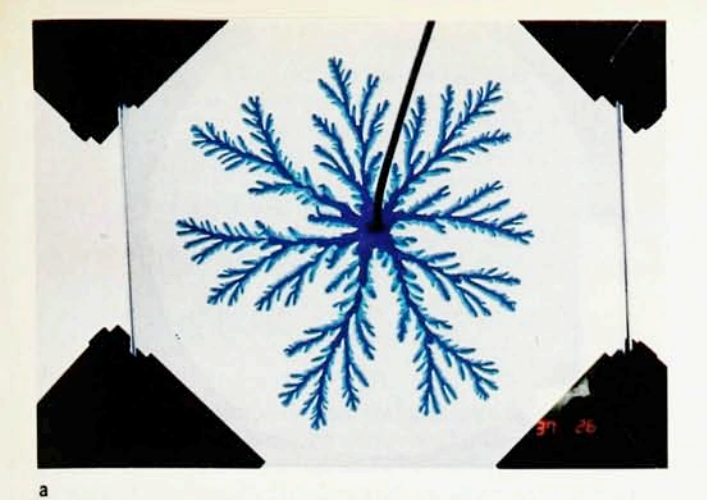
Po-zen Wong wrote this article while he was a research scientist at Schlumberger–Doll Research in Ridgefield, Connecticut. He is now an associate professor of physics and astronomy at the University of Massachusetts at Amherst.

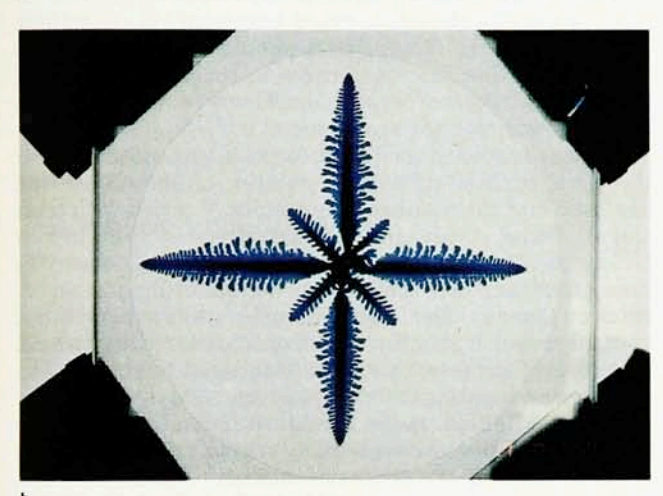
have caught my own fancy. They are by no means the only interesting or important ones, but they serve to illustrate how the modern theories of critical phenomena, percolation, diffusion-limited aggregation and dendritic growth are well suited for the study of rock.

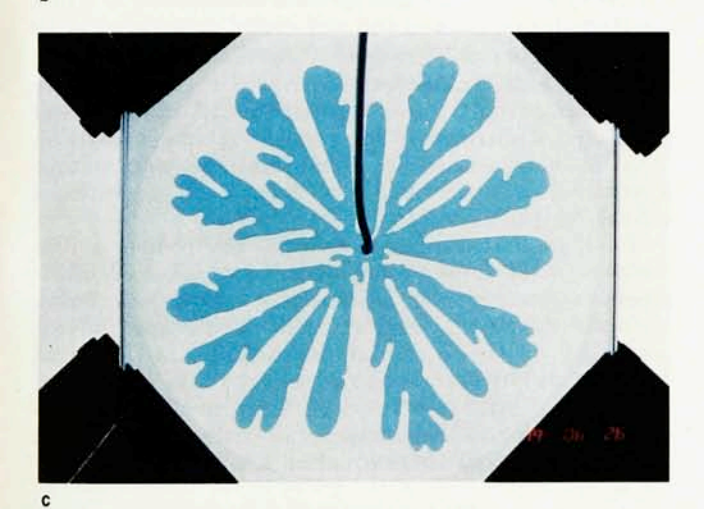
Grains, pores and fractals

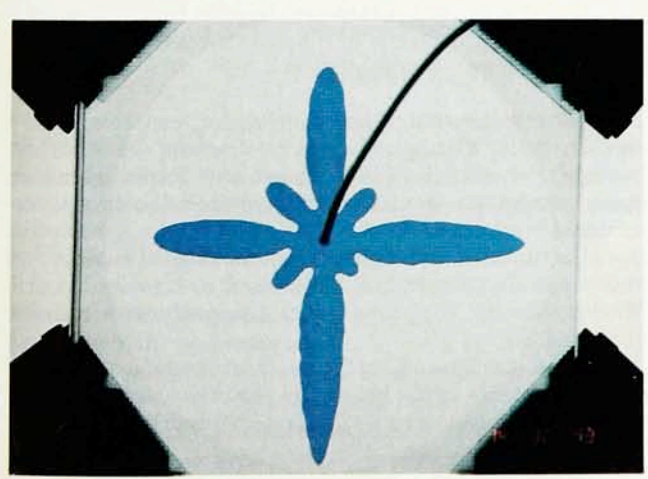
Perhaps the most obvious aspect of rocks that intrigues the statistical physicist is their microstructure. Figure 2a shows a scanning electron micrograph of a simple "clean" sandstone. We can see that it is just a random packing of sand grains of comparable sizes—grains of quartz typically tens to hundreds of microns in diameter. Such grains are sorted during sedimentation. After burial and compaction with other mineral sediments, they are consolidated under high pressure to form a rigid matrix with a multiply connected network of pores that controls how ions and molecules can move through the rock. Such ions and molecules in turn alter the rock over millions of years-a process called diagenesis. In figure 2b, which is a magnification of the central part of figure 2a, we can see a small amount of mineral that has grown on the grain surface with a highly irregular shape. Most sandstones are much "dirtier," containing much more of such minerals, the most common of which are clays formed of layered alumina silicate compounds.2 Figure 2c shows the intricate morphology of illite clay grown in the pores of a Coconino sandstone.

While a geologist would consider the sandstones in figure 2 to be simple, a physicist would study them with even simpler models. For example, we may use a dense random packing of glass beads of a single diameter, such as those shown in figure 3a, to mimic the grains in figure 2a. The porosity, or pore volume fraction ϕ , of such a packing of beads is about 40%, comparable to that of unconsolidat-









Viscous fingering patterns in a thin gap between two glass plates, formed as a less viscous fluid displaces a more viscous one at a high flow rate. 15 a: The miscible liquids water and glycerine interact in a Hele-Shaw cell. There is no surface tension between the two fluids, and a diffusion-limited aggregation structure with fine branches appears. b: A square lattice of grooves etched into the glass plates imposes an anisotropy, turning the random branching into regular branching as in a snowflake. c, d: The same setup as in a and **b** but with oil invading glycerine. The same patterns appear, except the fingers are much wider because of surface tension between the immiscible fluids. In a typical reservoir where water or gas displaces oil, the same kinds of fingering phenomena occur, leaving most of the oil in the ground. (Photographs courtesy of J.-D. Chen, Mead Imaging.) Figure 1

ed sand. We can sinter the beads to obtain the lower porosities that occur in rocks, and we can vary the grain size or make samples with mixtures of grain sizes. Such "toy rocks" have become known as Ridgefield sandstones and have many properties similar to those of real rocks.³

A perturbation on the packed-spheres model uses the concept of the fractal⁴ to describe the random mineral overgrowth seen in figures 2b and 2c. Figures 3b and 3c show two simple examples. The object in figure 3b is called a Koch island and is an example of a surface fractal. One begins with an equilateral triangle of side length L and then successively attaches smaller and smaller triangles of sizes L/3, $L/3^2$ and so on to the middle of every straight segment of the perimeter. After n iterations, the perimeter consists of N segments of length r, where $r = L/3^n$ and

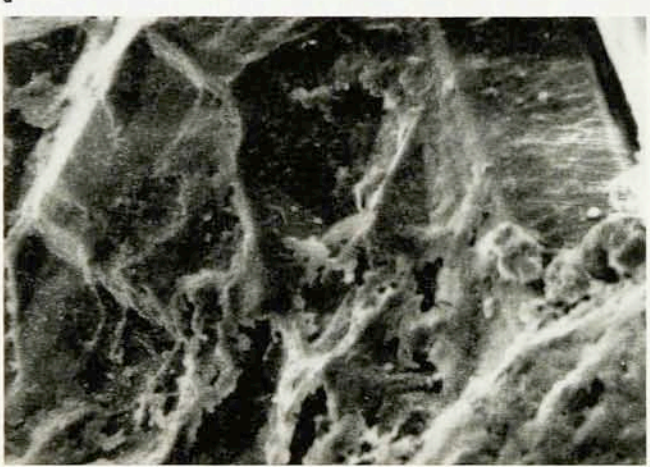
$$N = A(L/r)^{d_f} \tag{1}$$

The exponent $d_{\rm f}$ is called the fractal dimension, and A is a constant of order unity. For the Koch island, A is 3 and $d_{\rm f}$ is log $4/\log 3$, or about 1.262. This mathematics can be used to model the pores in a rock because ever-smaller mineral particles can grow or deposit on particles already present. When a pore of size L is observed with a resolution r, the number of surface features will be given by equation 1, and the measured surface area S by

$$S = Br^{2}(L/r)^{d_{\mathbf{f}}} = BL^{2}(L/r)^{d_{\mathbf{f}}-2}$$
 (2)

Figure 3c is an example of a volume, or mass, fractal called the Sierpinski gasket. Here, too, one begins with a triangle of side L to represent a smooth pore, but one then cuts out successively smaller triangles of sizes L/2, $L/2^2$ and so on to represent ever-smaller grains filling up the pore volume and reducing the porosity. After n iterations,







Sandstone as seen with an electron microscope. **a:** A 2.5-mm-wide region of a sample from Fontainebleau, France. **b:** A 0.05-mm-wide region of the same sample. **c:** Illite clay in a Coconino sandstone, at about the same magnification as in **b. Figure 2**

the pore space consists only of triangles of size r, given by $L/2^n$, and the number of such triangles is given by equation 1 with the constant A equal to 1 and the fractal dimension $d_{\rm f}$ equal to $\log 3/\log 2$, or about 1.585. Because a pore of size r contributes a porosity of order $(r/L)^3$, the total porosity is

$$\phi = C(L/r)^{d_f-3} \tag{3}$$

The pores in actual rocks behave differently from the

surface and volume fractals described above because they have random surface and volume elements with a continuous hierarchy of sizes between an upper limit L and an lower limit r. Equations 1–3 are applicable as representing statistical average behavior between these limits. The fractal dimension $d_{\rm f}$ should always be between 2 and 3 for either the pore surface or the pore volume. At least three types of experiments now support such a fractal description for sandstone:

The earliest work used an absorption technique to cover the pore surface with a monolayer of molecules and analyzed how the number of molecules N varied with their size r. David Avnir and his coworkers at the Hebrew University of Jerusalem⁵ found that equation 1 describes many rock and soil samples with fractal dimensions d_i between 2 and 3. The length scales probed by this method typically range from a few angstroms to tens of angstroms. Arthur Thompson and his colleagues at Exxon Production Research performed digital image analyses on micrographs similar to those in figure 2 and studied the distribution of feature sizes along straight lines across the picture.6 A sharp peak in the intensity signals an edge, and two neighboring edges define a feature size r. From equation 1, one expects the size distribution $N_1(r)$ to be proportional to $r^3(\mathrm{d}N/\mathrm{d}r)$, or $r^{2-d_{\mathrm{f}}}$, and Thompson and his coworkers indeed observed this in sandstones with pore sizes ranging from 0.1 microns up to the typical pore size of a few tens of microns. In some rocks that are severely altered by diagenesis, they found that the pore volume distribution was consistent with equation 3, suggesting a volume-fractal behavior.

 \triangleright Small-angle scattering of thermal neutrons or x rays has been used in recent years to study a wide variety of disordered systems such as polymer gels, aggregated colloids, oil-water emulsions and cements. The reason is that according to the Born approximation, the scattered intensity, or cross section, as a function of the wavevector transfer, I(q), is just the Fourier transform of the density-density correlation that characterizes the structure. For a surface fractal that obeys equation 2, one finds

$$I(q) \propto q^{-(6-d_{\mathbf{f}})} \tag{4}$$

For a volume fractal, however,

$$I(q) \propto q^{-d_q}$$
 (5)

The different powers of the wavevector q in equations 4 and 5 readily distinguish volume fractals from surface fractals, because $d_{\rm f} \! \leqslant \! 3$ and $6-d_{\rm f} \! \geqslant \! 3$. Experiments on many sandstones and shales have found behavior described by equation 4. A log-log plot of the wavevector transfer function I(q) (figure 4) shows slopes between -3 and -4, indicating fractal dimensions $d_{\rm f}$ between 2 and 3. The length scale 1/q probed by these experiments is under about 500 Å.

These studies indicate that fractal surface behavior spans all length scales below the pore size. An important open question concerns the unknown growth mechanisms Geometrical models for sedimentary rocks.

a: Dense random packing of 0.2-mm-diameter glass spheres models the packing of clean sand grains in sandstone. b: Koch island with a fractal perimeter models a pore with a fractal or rough surface. c: Sierpinski gasket models a set of tiny pores that link up to form a fractal volume. Figure 3

responsible for the observed wide range of fractal dimensions. There is only a clue at present. We know that clay compounds tend to incorporate into their lattices many impurity ions with the "wrong" valences, and that the excess charge is balanced by counterions adsorbed onto the surface. In addition, water molecules tend to be adsorbed because of their dipolar nature. As a result of such adsorption processes the system tends to maximize the surface area, and one may consider the growth to be driven by a negative surface tension. This mechanism is called antisintering.⁸

Porosity and conductivity

Now that we have some simple ideas about pore geometry, we can consider the movement of ions and molecules in the random medium. One common hypothesis is that the pores are always connected, even if they do not seem to be. The reason is that the pores are altered by the fluids that flow through them. As they become smaller, less fluid can flow and less alteration can occur. This is much like saying that a clogged kitchen sink is never perfectly clogged, it just drains very very slowly! Fluid flow and electrical conduction should exist even as the porosity ϕ tends to zero. In the theorist's jargon, we can say that rocks have a zero percolation the shold.

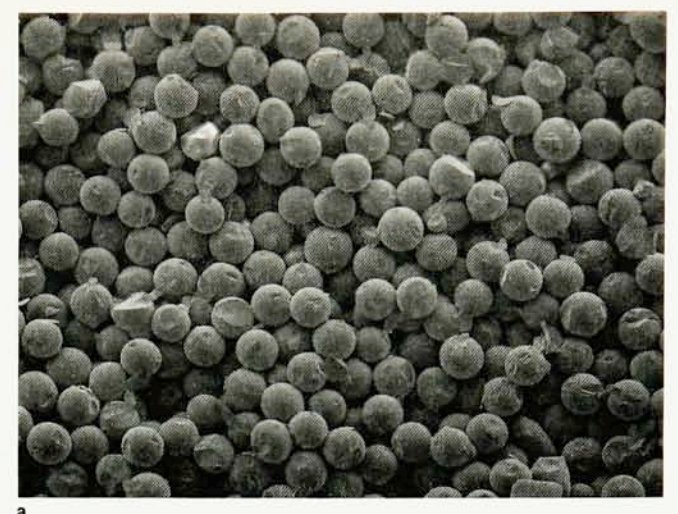
The conductivity σ_r of water-saturated rock is often estimated by the empirical Archie's law⁹:

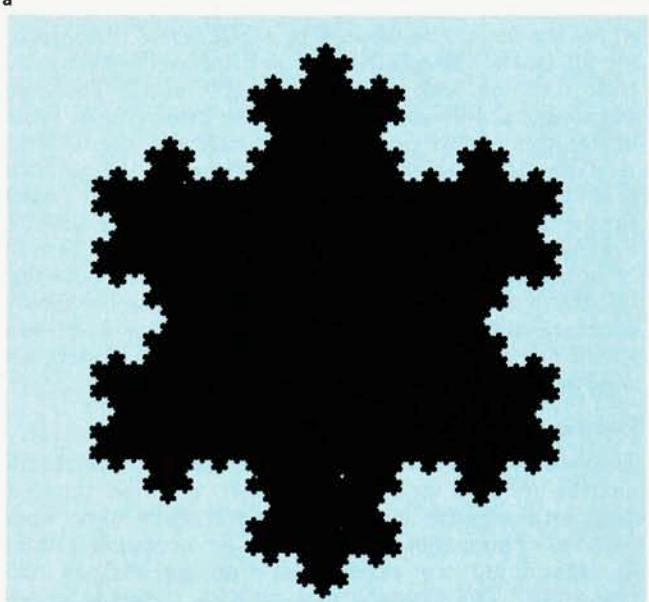
$$\sigma_r = \sigma_w / F \approx a \sigma_w \phi^{-m} \tag{6}$$

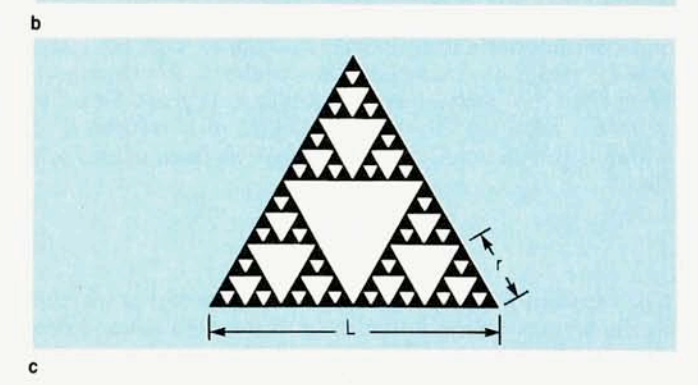
Here $\sigma_{\rm w}$ is the conductivity of water and F is the formation factor, which characterizes the transport geometry. Figure 5 shows that data for 52 rocks and 12 Ridgefield sandstones roughly follow this expression with a and m equal to 0.8 and 2, respectively. There have been many attempts to understand this behavior. Two simple models have proved to be the most illuminating

have proved to be the most illuminating. The first is the "shrinking tube" model, which exploits the analogy with percolation theory. In ordinary bond percolation, the conductive bonds in a network are snipped off at random. The network becomes disconnected as the bond fraction p reaches a threshold p_c . For $p \ge p_c$, the conductivity approaches zero asymtotically as $(p-p_c)'$. The critical exponent t is about 1.9. This expression is similar to Archie's law if we identify the bond fraction p with the porosity p and assume that the threshold p_c is 0.

Operationally, the shrinking-tube model takes a simple cubic network of tubes with a uniform radius r_0 and reduces the radii randomly by a factor α rather than cutting them off as in percolation. By keeping track of how the porosity and conductivity vary, one finds that Archie's law is obeyed exactly in this model, with $m = (\ln \alpha^2)/(\alpha^2 - 1)$ and $0 < \alpha < 1$. This result derives from the fact that the porosity scales as the average conductance, which is proportional to $\langle r_i^2 \rangle$, or $\langle \alpha^{2n_i} \rangle$, and is weighted heavily by the few large tubes, whereas the conductivity for a fully connected network scales with its most probable conductance, which is proportional to $\alpha^{2\langle n_i \rangle}$.







In other words, Archie's law comes from the fact that the porosity and conductivity are influenced by different parts of a skewed "pore size" distribution. A large value of the exponent m implies that there are large pores that contribute little to the conduction.

The difficulty in applying the shrinking-tube model to real rocks is the mapping of a random pore space into a simple network, because there is no simple algorithm for transforming an irregularly shaped pore into an equivalent tube. In this respect the "grain consolidation" model invented by James Roberts and Lawrence Schwartz of Schlumberger–Doll Research is very helpful.¹¹ Roberts and Schwartz began with a computer model of the dense random sphere packing (figure 3a) and constructed

Wigner-Seitz-like cells, called Voronoi polyhedra, for each sphere. The vertices of the polyhedra are identified with the nodes of the network, and the edges are the bonds. The spheres are then allowed to grow uniformly to create larger contact areas with neighboring spheres, thus mimicking the consolidation process. By keeping track of how the porosity and conductivity decrease together, Roberts and Schwartz found that Archie's law is obeyed approximately over much of the porosity range of practical interest. The reason the grain-consolidation model works is similar to the reason the shrinking-tube model works: The porosity is due mainly to the open regions around the nodes, while the conductances are controlled by the narrow "throats" of the bonds. Figure 5, which shows the formation factor F as a function of the porosity for this model, demonstrates that the model describes the rock data as well as Archie's law does. The only significant difference is that for the grain-consolidation model the critical porosity at which the conductivity vanishes is finite-about 3.65%-because the uniform grain growth closes off the throats before the radii reach the vertices of the Voronoi polyhedra. Because most rocks of practical interest have higher porosities, this difference is unimportant. On the other hand, we should note that the above description of conductivity neglects the mobile counterions on the fractal clay surface. This involves a whole new set of problems, and interested readers are referred to reference 7 for a brief discussion.

Permeability and length scales

The merits of the shrinking-tube and grain-consolidation models are not so much that they describe the real diagenetic processes as that they capture some basic features of pore geometry and provide a common ground for examining the relationships among various rock properties. The network picture gives a simple understanding of the formation factor F. In both models, there is a characteristic bond length that scales with the grain size $l_{\rm g}$, and a characteristic throat size $l_{\rm t}$ for transport. Hence the characteristic conductance $g_{\rm r}$ is proportional to $\sigma_{\rm w} \, l_{\rm t}^2 / l_{\rm g}$. Because the conductance $g_{\rm w}$ of a volume $l_{\rm g}^3$ of water is proportional to $\sigma_{\rm w} \, l_{\rm g}$, it follows from equation 6 that

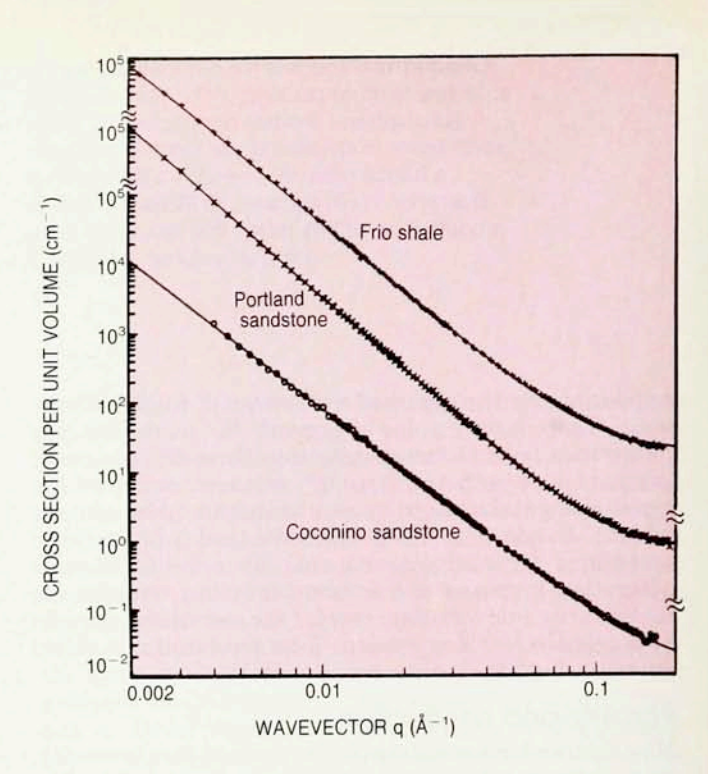
$$F = \frac{g_{\rm w}}{g_{\rm r}} = \beta \frac{l_{\rm g}^2}{l_{\rm t}^2} \tag{7}$$

The constant β is related to such nonuniversal properties as the bond coordination number of the network and how the effective bond length scales with the actual grain size.

The concept of throat size has been refined by David L. Johnson and his coworkers at Schlumberger-Doll Research¹² as a weighted volume-to-surface ratio called Λ , given by

$$\Lambda \equiv 2 \frac{\int |E_0|^2 \mathrm{d}V_p}{\int |E_0|^2 \mathrm{d}S_p}$$

Here $V_{\rm p}$ and $S_{\rm p}$ are the pore volume and the pore surface, respectively, and E_0 is the electric field in the rock in the absence of a permanent surface charge. Because the weighting factor $|E_0|^2$ is largest in the narrowest throats, Λ is an effective throat size. In the grain-consolidation model, for example, Schwartz has shown that the formation factor is proportional to Λ^{-2} for porosities far from the critical porosity, in agreement with equation 7. Near



Neutron scattering data for sandstone. The intensity of neutrons scattered at small angles shows the power-law behavior described by equation 4 plus a constant background. This behavior supports a fractal pore-surface picture below 500 Å. Figure 4

the critical porosity, Λ becomes dependent on how the throats are connected.

Using the network picture and equation 7, we can easily describe how a single fluid flows through porous rock. We recall that for Poiseuille flow through a cylindrical pipe of radius R, the flow rate is given by

$$\stackrel{\cdot}{Q}=\frac{\pi R^4}{8\mu}|\nabla P|$$

Here μ is the viscosity of the fluid and ∇P is the pressure gradient. Now if we fill the pipe with grains of size $l_{\rm g}$, then the number of small throats running in parallel through a cross section of the pipe will be proportional to $R^2/l_{\rm g}^2$, so that the flow rate becomes

$$\dot{Q}_{
m r} \propto rac{\pi (R^2/l_{
m g}^2) l_{
m t}^4}{8 \mu} |
abla P|$$

Dividing through by πR^2 gives the well-known Darcy's law, an analog of Ohm's law, for the effective flow velocity:

$$\mathbf{v} = -\frac{k}{\mu} \nabla P \tag{8}$$

The factor k is an analog of the conductivity called the permeability and is given by

$$k \propto l_t^4 / l_\sigma^2 \tag{9}$$

The permeability can be related to the grain size or throat size by combining equations 7 and 9:

$$k = c_1 l_\sigma^2 / F^2 (10)$$

$$k = c_2 l_t^2 / F \tag{11}$$

The factors c_1 and c_2 are dimensionless constants. These relationships are based on the simple pictures of the shrinking-tube and grain-consolidation models: The rock

has a well-defined grain size; the network is well connected and can be replaced by the most probable bond. Equations 10 and 11 have been tested out on both Ridgefield standstone and real rock.^{3,6} The experiments have found that the prefactors c_1 and c_2 are approximately 0.01.

Although equations 10 and 11 are derived only heuristically, they can be justified by percolation theories. Bertrand Halperin at Harvard University and his coworkers have studied a "Swiss cheese" model in which the holes are like the sand grains and the cheese is like the pore water. If we make more and more holes, the cheese fraction ϕ approaches a threshold ϕ_c at which the conductivity vanishes as F^{-1} , or $(\phi-\phi_c)^{\bar{t}}$, and the permeability vanishes as $(\phi-\phi_c)^{\bar{t}}$. The exponents \bar{t} and \bar{e} are found to be about 2.4 and 4.4, respectively, giving a permeability proportional to $F^{-\bar{t}/\bar{t}}$, or about $F^{-1.8}$, which is nearly the same as the noncritical F^{-2} behavior in equation 10.

Alan Katz, now at Texas Instruments, and Thompson use a clever mercury injection method⁶ to determine l_t in equation 11. They monitor the resistance across each sample while applying pressure to force mercury into the pores. Because mercury is a nonwetting fluid, it can pass a throat of size l_t only if the pressure exceeds a capillary pressure of order γ/l_t , where γ is the surface tension. At some critical pressure P_c , the injected mercury forms a percolating path across the sample and is detected by a sharp drop in the resistance. This defines a critical throat size l_c that can be used in equation 11.

Viscous fingering

Having understood how water flows through rock, we can now proceed to discuss how oil and water displace each other. Hydrocarbons are generated at a "source rock" by the decay of organic matter in an oxygen-deficient environment. Because of their low densities, hydrocarbons migrate along permeable beds in a generally upward direction until they are trapped by geological structures made of low-permeability "cap rock." The region of the trap is called "reservoir rock" and always contains both water and oil. The determinations of the oil saturation S_0 and water saturation $S_{\rm w}$ in the reservoir and their relative permeabilities k_o and k_w are among the most important rock physics problems for oil companies. The product ϕS_o tells them how much money (in oil and gas) they have in reserves, while kk_o tells them how fast the money can be withdrawn. While ϕ and k are intrinsic properties of the rock, S_o and k_o depend on how the oil and water are distributed and move through the pores. The fundamental problem here is to understand how various patterns develop as an invader fluid displaces a defender fluid. Some of the most interesting patterns can be observed in a Hele-Shaw cell where a low-viscosity invader displaces a high-viscosity defender in a thin gap between two glass plates.14 Figure 1 shows some beautiful examples.15

Figure 1a is a displacement pattern of miscible fluids, namely water (dyed blue) invading glycerine. The fractal branching structure is similar to that obtained by diffusion-limited aggregation. The reason is believed to be that both phenomena are approximately described by a Laplace equation. In diffusion-limited aggregation, the growth is controlled by a density field u that obeys the diffusion equation

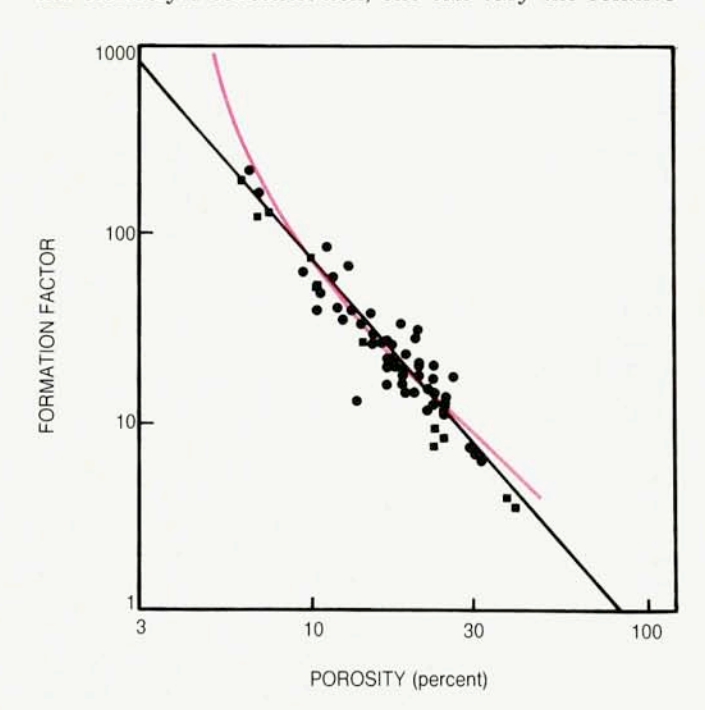
$$\nabla^2 u = \frac{1}{D} \frac{\partial u}{\partial t} \approx \frac{1}{D} \mathbf{v} \cdot \nabla u \tag{12}$$

If the growth is slow enough that the diffusion length $l_{\rm D}$, defined as D/v, goes to infinity, then this expression reduces to $\nabla^2 u=0$. In the Hele–Shaw problem, the velocity field ${\bf v}$ obeys equation 8 with $k=b^2/12$, where b is the gap size. In the limit that the pressure field P varies mainly in the defender, one finds that

$$abla^2 P \approx \frac{\kappa \mu}{k} \mathbf{v} \cdot \nabla P$$

Here κ is the defender's compressibility. By comparison with equation 12 one finds an equivalent diffusion length $l_{\rm eq}$, equal to $k/\mu\kappa v$, which for typical experimental conditions is longer than a kilometer. So the fluids can be considered incompressible and $\nabla^2 P=0$.

The same analogy applies to many other systems, the most notable one being the growth of snowflakes. There the latent heat of solidification has to diffuse away from the seed crystal, and the temperature field T obeys the equation $\nabla^2 T = 0$. The difference is that a snowflake has well-ordered dendrites due to its crystalline anisotropy. If one etches a square network of uniform grooves into one of the Hele–Shaw plates, a giant snowflake pattern is easily obtained (figure 1b). Another well-known example is the electrochemical deposition of metal through an aqueous electrolyte. There the electrostatic potential $\Phi_{\rm e}$ and the concentrations c_{\pm} of positive and negative ions combine to give the chemical potentials Φ_{\pm} , given by $q_{\pm}\Phi_{\rm e}+k_{\rm B}T\log c_{\pm}$, where the q_{\pm} are the charges of the ions, and $\nabla^2\Phi_{\pm}=0$. By adjusting the applied voltage and the electrolyte concentration, one can vary the relative



Formation factors for 52 real rocks (circles) and 12 "toy rocks" made of fused glass beads (squares). Both types of rock are roughly described by the empirical Archie's law, equation 6, with the exponent *m* equal to 2 (straight line). The colored curve represents results of the grain-consolidation model calculation. **Figure 5**

29

strengths of the two terms in the expression for $\Phi_\pm\,$ and observe a transition from a diffusion-limited aggregation

pattern to a dendritic pattern.

Surface tension. In the case of oil and water, which as we all know do not mix, we must consider another factor: the surface tension γ . The immiscibility has two important effects. First, it suppresses the branching structure at short length scales.¹⁷ Figures 1c and 1d show the displacement patterns of immiscible fluids, namely oil invading glycerine. These patterns have the same general character as those in figures 1a and 1b except that the fingers are much wider. The reason for this is that the creation of a bump of size l in d dimensions costs a surface energy γl^{d-1} but saves a volume energy $\Delta P l^d$, where ΔP is the pressure drop across the system. Hence the bump size must be greater than $\gamma/\Delta P$, which is defined as the capillary length $l_{\rm ca}$ and sets a minimum size for the finger width. In more general cases, there are other mechanisms that further increase the finger width. For example, in the growth of a snowflake, the diffusion length l_{D} characterizes the decay of the temperature field away from the interface; the spreading of the associated heat current smooths out the interfacial structure and gives a finger width of approximately $(3l_{\rm D}l_{\rm ca})^{1/2}$. In the Hele-Shaw cell, because the equivalent diffusion length $l_{\rm eq}$ is much larger than the cell, the size and shape of the cell and the wettability of the plates become important factors.14

The second important effect of surface tension is that it creates capillary forces on the tiny oil–water menisci in the pores. Putting aside the fractal nature of the pore surface, the meniscus perimeter scales with the grain size $l_{\rm g}$ and its area scales as $l_{\rm t}^2$. Thus the interfacial pressure $\Delta P_{\rm y}$ is proportional to $\gamma l_{\rm g}/l_{\rm t}^2$. The viscous pressure drop $\Delta P_{\rm vis}$ across a grain is proportional to $l_{\rm g}\,\nabla P$, or $l_{\rm g}\mu v/k$, so the ratio $R_{\rm ye}$ of the interfacial pressure to the viscous pressure is approximately 19

$$\gamma k/\mu v l_{\rm t}^2 = k'/N_{\rm ca}$$

Here k' is defined as $k/l_{\rm t}^2$ and $N_{\rm ca}$, called the capillary number, is defined as $\mu v/\gamma$. In real rock, k' is typically less than 10^{-3} . Because a typical flow velocity v in a reservoir is about 1 ft/day, or 4 microns/sec, $N_{\rm ca} < 10^{-6}$, $R_{\gamma v} > 10^3$ and the viscous pressure has little effect at length scales below a characteristic value $l_{\rm cv}$ given by $l_{\rm g}R_{\gamma v}$. This characteristic length $l_{\rm cv}$ defines a crossover length between capillary and viscous effects and is typically on the order of 1 meter. Viscous fingering is, therefore, a large-scale reservoir phenomenon.

Invasion percolation

Below the crossover length, the interfacial pressure ΔP . becomes the dominant driving force. It is clear that if the invader is the wetting fluid, it will first go into the smallest pores. Conversely, if the invader is the nonwetting fluid, it will first go into the largest pores. It is believed that sandstones are often water wet, and carbonate rocks oil wet. To simulate this invasion process on a network, one can assign a random number to every bond and select bonds sequentially to represent the invaded pores. If the selection follows the order of the random numbers, then it is just the ordinary bond percolation. If, however, one selects the most favorable bond at the invasion front, then one obtains the invasion percolation model.20 This model ensures that the invader flows along a continuous path, but it allows the defender to be completely surrounded and form a trapped cluster.

An experimental demonstration of these effects uses a two-dimensional network of random ducts etched into a glass plate.20 Figure 6 shows a pattern that Roland Lenormand, now at Institut Français du Petrole, obtained by slowly injecting air into paraffin oil in a 350×350 network, a nonwetting invasion. The connected white area in the photograph is the air, and the disconnected black patches are the trapped oil. The pattern is visually very different from those in figure 1, created by viscous forces, but both are fractals. An analysis of the invader cluster in figure 6 gives a fractal dimension d_f of about 1.8, which is slightly different from the value of 1.9 for the infinite cluster in ordinary two-dimensional percolation.20 However, this difference turns out to be an artifact of the two-dimensional square lattice, because only one phase can form an infinite cluster. For a real, three-dimensional rock, it is generally believed that invasion percolation is basically the same as ordinary bond percolation except that the invader can only move on the infinite cluster. As a result, the threshold for the invader occurs at zero saturation, while that for the defender occurs at a nonzero value called the irreducible saturation, at which the defender is broken up into immobile clusters. This is one of the main reasons why a large fraction of the hydrocarbons in a reservoir is not easily producible.

To assess the oil and water saturations in a reservoir, a common practice is to measure the rock conductivity and assume a modified Archie's formula⁹:

$$\sigma_{\rm r} = \sigma_{\rm w} \, \phi^m S_{\rm w}^n$$

The exponent n is often taken to be the same as m. The foundation of this formula is weak, however, because the distribution of oil and water in the pore is known to be dependent on history. The water pattern at any saturation $S_{\rm w}$ depends on both the initial state and the rate at which it is changed. One assumes that over geological times the

change is quasistatic.

In the laboratory, the growth of such a fractal cluster very time consuming, and if it is not properly equilibrated at the start of an experiment, all subsequent data points can be meaningless. The mercury injection experiment of Thompson and his coworkers demonstrated the effects very nicely.6 By performing slow measurements with high precision, they found that the injected volume undergoes a small first-order jump as the mercury forms a connected cluster across the rock at a critical pressure (figure 7a). Thereafter the resistance of the sample decreases through an infinite number of steps like a "Devil's staircase" as the pressure is increased (figure 7b). (See Per Bak's article "The Devil's Staircase," Physics TODAY, December 1986, page 38.) For each small step in pressure, the resistance approaches a new equilibrium value according to a stretched exponential relaxation that takes many hours. The total number of equilibrium resistance steps larger than ΔR follows a power law $\Delta R^{-\lambda}$, where $\bar{\lambda}$ varies between 0.57 and 0.81 for various rocks.

It turns out that at least the static behavior is understandable in terms of invasion percolation. Because the mercury can only occupy the infinite cluster and leaves all the disconnected clusters empty, its advance in one bond can make a large disconnected cluster behind it accessible. Because the experiment is carried out at constant pressure rather than constant flow rate, the mercury can invade the entire cluster once it becomes accessible, and clearly the largest clusters occur near the threshold. Both computer simulation studies and scaling analyses so that such a cluster-by-cluster invasion mechanism would give a resistance staircase with $\bar{\lambda}$ in good agreement with experiment.



Gravity and wettability. In applying the invasion

percolation concept to oil and water in a real reservoir, there are two important complications. The first has to do with the density difference $\Delta \rho$ between oil and water. 19 This difference creates a gravitational pressure gradient $abla P_{g}$ between the two phases and hence a vertical saturation gradient, so the lighter oil will have a higher saturation near the top of the reservoir. The transition between oil and water zones takes place over a height h given approximately by $\Delta P_{\gamma}/\nabla P_{\mathrm{g}}$. To represent this effect in a percolation model, one would include a bond concentration gradient ∇p proportional to 1/h. The ratio $l_{\rm g}/h$ is called the Bond number $N_{\rm B}$. (For a packing of 100-micron spheres, $N_{\rm B}$ is of order 10^{-4} .) David Wilkinson of Schlumberger-Doll Research has pointed out 19 that such a gradient destroys the critical behavior of percolation, because the correlation length ξ normally diverges as $l_{\rm g}(p-p_{\rm c})^{-\nu}$ and the gradient makes it impossible for $p-p_c$ to be less than $\xi \nabla p$. As a result, $(\xi/l_g)^{-1/\nu} < \xi N_B/l_g$

$$\xi < l_g N_B^{-\nu/(1+\nu)} \equiv \xi_{\text{max}}$$

This is actually a general result for all critical phenomena with an imposed gradient. For example, a thermal gradient on a ferromagnet would cut off the correlation length divergence at the Curie temperature, but the effect is often difficult to observe. Here, however, because ν is about 0.8 for three-dimensional percolation, the exponent v/(1+v) is about 0.47 and $\xi_{\rm max}$ is only a few hundred times $l_{\rm g}$, or a few centimeters. Because $\xi_{\rm max}$ is the size of the largest blob of trapped fluid, this smearing of the percolation critical point has the fortunate consequence that we can extract more oil in the presence of gravity than we could without it. It also explains the jump in mercury saturation in figure 7, because the volume fraction of a percolation cluster of size $\xi_{\rm max}$ is of order $(\xi_{\rm max}/l_{\rm g})^{d_{\rm f}-3}$, which is about 10% or less; $d_{\rm f}$, the fractal dimension of the percolation cluster in three dimensions, is about 2.5.

The second complication of invasion percolation has to do with wetting effects. Lenormand pointed out that

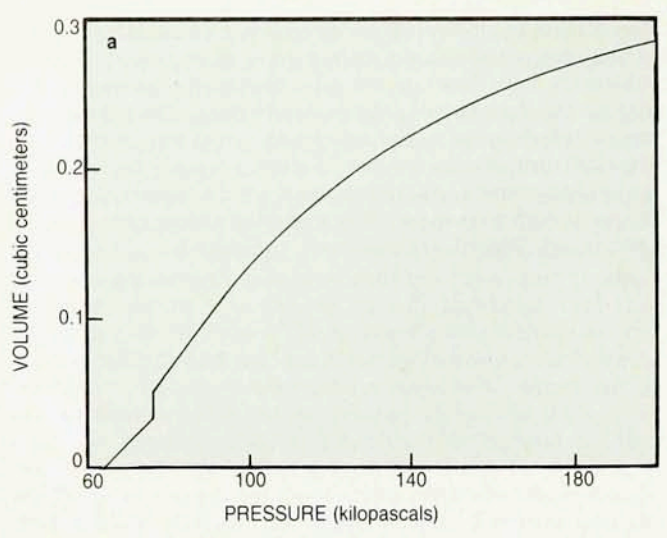
Percolation of air through paraffin oil in a 350×350 network of randomly sized grooves etched into a glass plate.²⁰ At a sufficiently slow flow rate, the oil is displaced pore by pore through the invasion percolation mechanism. The light area is the air, which forms a connected path across the sample. The dark regions are immobile, disconnected patches of trapped paraffin oil. Such trapping is a major cause of low oil recovery from a reservoir. (Photograph courtesy of R. Lenormand, Dowell-Schlumberger.) Figure 6

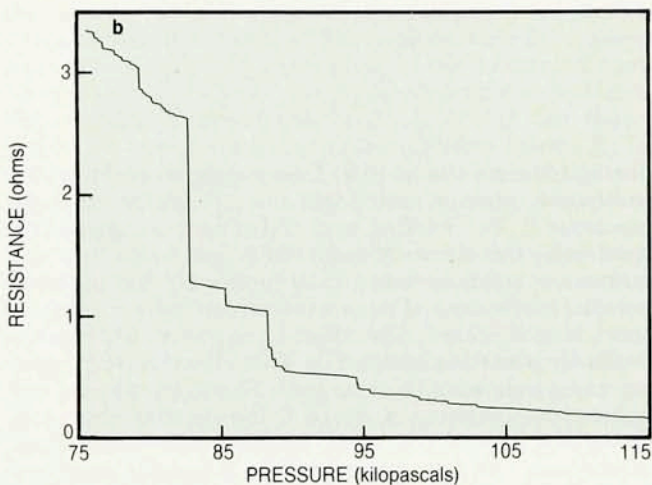
during invasion the menisci from neighboring ducts can touch each other on their edges and collapse into a single meniscus.20 For wetting and nonwetting invasions, respectively, this draws invader fluid into pores that are larger or smaller than those predicted by invasion percolation theory and smears the percolation structure at short length scales. The effect is expected to be more severe for a wetting invasion, in which the menisci's edges are always ahead of their centers. However, even for the nonwetting invasion in figure 6 the invader cluster is essentially compact at short length scales due to this mechanism. An interesting question is how the crossover from compact to fractal structures depends on the contact angle Θ , which is a measure of the wettability.

Experimental and theoretical studies of this problem have recently been carried out for systems that are more like real rock. A group led by James Stokes and David Weitz of Exxon Research and Engineering put glass beads in the gap of a Hele-Shaw cell to conduct both wetting and nonwetting invasion experiments.22 By choosing the proper capillary number, they made the crossover length l_{cv} somewhere between the cell size and the grain size so that they could observe both viscous fingering and invasion percolation patterns. While this was indeed what they saw in the nonwetting invasion runs, they found that wetting invasion runs gave compact fingers with average widths that cannot be explained easily by any existing theory. On the theoretical side, Marek Cieplak and Mark Robbins of Johns Hopkins University have carried out a two-dimensional simulation using random circles to represent the grains, and the spaces between them the pores.23 They found that the invader pattern is compact below a size \overline{W} that depends on the contact angle Θ . In the entire nonwetting invasion regime, for which Θ is greater than 90°, the size \overline{W} is about five lattice constants, which is consistent with the experiments. However, in the wetting invasion regime, for which Θ is less than 90°, the size \overline{W} appears to diverge at a critical contact angle Θ_c as $(\Theta - \Theta_c)^{-2.3}$, suggesting a critical phenomenon.

The studies of viscous fingering and invasion percolation on model systems discussed above may seem academic to some, but the practical implications of such understanding are enormous. In a typical producing reservoir water or gas displaces a more viscous oil. So on length scales

31





larger than l_{cv} , the fractal viscous fingering pattern (figure 1a) leaves large regions of oil untapped. Even below l_{cv} , the invasion percolation trapping mechanism leaves behind large blobs of oil of size ξ_{max} within the fingers where oil is displaced (figure 6). As a result, most of the oil is left in the ground: Common estimates24 for recovery efficiencies range from 5% to 50%. To overcome this problem, one would have to optimize the operating parameters of the reservoir. For example, making l_{cv} as large as possible will reduce the fingering effect, and modifying the wettability with chemicals to ensure $\Theta < \Theta_c$ will minimize the percolation effect. Because the crossover length l_{cv} is inversely proportional to the flow velocity v, an anxious oil producer who speeds up pumping for a short-term gain will make most of the oil unproducible. Understanding the basic science, on the other hand, will result in a better long-term gain.24

I found the quote that begins this article in E. Courtens, R. Vacher, Zeitschrift für Physik B 68, 355 (1987). I thank E. Courtens for sending me the reprint.

I am grateful to my friends at Schlumberger-Doll Research for stimulating my interest in rock physics. It has truly been a great pleasure to have learned from and worked with them over the last six years. I hope this article will preserve some of the good spirit and fond memories we share.

References

 J. R. Banavar, J. Koplik, K. W. Winkler, eds., Physics and Chemistry of Porous Media II, AIP Conference Proceedings 154, AIP, New York (1987). Mercury injection experiment results.⁶ The very slow injection of mercury into a rock helps in the study of the invasion percolation mechanism. The plot of injected volume as a function of pressure shows a first-order jump as the mercury forms a connected cluster (a). Thereafter, the resistance of the sample descends through a Devil's staircase (b). Both phenomena can be explained by invasion percolation with a gravitational pressure gradient. Figure 7

- J. E. Welton, SEM Petrology Atlas, American Association of Petroleum Geologists, Tulsa, Okla. (1984).
- P.-z. Wong, J. Koplik, J. P. Tomanic, Phys. Rev. B 30, 6066 (1984).
 E. Guyon, L. Oger, T. J. Plona, J. Phys. D 20, 1637 (1987).
- B. B. Mandelbrot, The Fractal Geometry of Nature, Freeman, San Francisco (1982).
- D. Farin, D. Avnir, in *Characterization of Porous Solids*, K. K. Unger, D. Behrens, H. Kral, eds., Elsevier, Amsterdam (1988), and references therein.
- A. H. Thompson, A. J. Katz, C. E. Krohn, Adv. Phys. 36, 625 (1987), and references therein.
- P.-z. Wong, in J. R. Banavar, J. Koplik, K. W. Winkler, eds., Physics and Chemistry of Porous Media II, AIP Conference Proceedings 154, AIP, New York (1987), p. 304. For a review of the scattering theory and references for various applica- tions, see P.-z. Wong, A. J. Bray, Phys. Rev. B 37, 7751 (1988); J. Appl. Crystallogr. (1988), in press.
- See, for example, M. H. Cohen, in *Physics and Chemistry of Porous Media II*, AIP Conference Proceedings 154, J. R. Banavar, J. Koplik, K. W. Winkler, eds., AIP, New York (1987), p. 3.
- 9. G. E. Archie, AIME Trans. 146, 54 (1942).
- See, for example, S. Kirkpatrick, in *Ill-Condensed Matter*, R. Balian, R. Maynard, G. Toulouse, eds., North Holland, Amsterdam (1979).
- 11. J. N. Roberts, L. M. Schwartz, Phys. Rev. B 31, 5990 (1985).
- D. L. Johnson, T. J. Plona, H. Kojima, in *Physics and Chemistry of Porous Media II*, AIP Conference Proceedings 154, J. R. Banavar, J. Koplik, K. W. Winkler, eds., AIP, New York (1987), p. 243. D. L. Johnson, J. Koplik, L. M. Schwartz, Phys. Rev. Lett. 57, 2564 (1986).
- 13. B. I. Halperin, S. Feng, P. Sen, Phys. Rev. Lett. 54, 2391 (1985).
- See, for example, D. Bensimon, L. P. Kadanoff, S. Liang, B. I. Shraiman, C. Tang, Rev. Mod. Phys. 58, 977 (1986), and references therein.
- 15. J.-D. Chen, Exp. Fluids 5, 363 (1987).
- For a review, see L. Sander, Nature 322, 789 (1986); L. Sander, in *The Physics of Structure Formation*, W. Guttinger, G. Dangelmayr, eds., Springer-Verlag, Berlin (1987), p. 257.
- For a review, see D. A. Kessler, J. Koplik, H. Levine, Adv. Phys. (1988), in press.
- 18. R. M. Suter, P.-z. Wong, Phys. Rev. B (to be published).
- 19. D. Wilkinson, Phys. Rev. A 30, 520 (1984); 34, 1380 (1986).
- R. Lenormand, in *Physics and Chemistry of Porous Media II*,
 AIP Conference Proceedings 154, J. R. Banavar, J. Koplik,
 K. W. Winkler, eds., AIP, New York (1987), p. 98. R. Lenormand, C. Zarcone, Phys. Rev. Lett. 54, 2226 (1985). See also D. Wilkinson, J. Willemsen, J. Phys. A 16, 3365 (1983).
- 21. J.-N. Roux, D. Wilkinson, Phys. Rev. A 37, 3921 (1988).
- J. P. Stokes, D. A. Weitz, J. P. Gollub, A. Dougherty, M. O. Robbins, P. M. Chaikin, H. M. Lindsay, Phys. Rev. Lett. 57, 1718 (1986).
 D. A. Weitz, J. P. Stokes, R. C. Ball, A. P. Kushnick, Phys. Rev. Lett. 59, 2967 (1987).
- M. Cieplak, M. O. Robbins, Phys. Rev. Lett. 60, 2042 (1988).
- 24. See, for example, M. Gerding, ed., Fundamentals of Petroleum, Petroleum Extension Service, Univ. Texas, Austin (1981). For an overview of science and technology in the oil industry, see D. V. Ellis, Well Logging for Earth Scientists, Elsevier, New York (1987).